

MHD MATERIALS - SEED/SLAG INTERACTIONS AND EFFECTS

QUARTERLY PROGRESS REPORT

April - June 1980

Samuel J. Schneider
Project Manager

Center for Materials Science
U. S. Department of Commerce
National Bureau of Standards
Washington, D. C. 20234

PREPARED FOR THE UNITED STATES
DEPARTMENT OF ENERGY
MHD OFFICE

"This report was prepared as an account of work sponsored by the United States Government. Neither the United States nor the United States Department of Energy, nor any of their employees, nor any of their contractors, subcontractors, or their employees, makes any warranty, express or implied, or assumes any legal liability or responsibility for the accuracy, completeness, or usefulness of any information, apparatus, product or process disclosed, or represents that its use would not infringe privately owned rights."

TABLE OF CONTENTS

| | <u>Page</u> |
|--|-------------|
| I. SUMMARY OF PROGRESS TO DATE. | 1 |
| II. DETAILED DESCRIPTION OF TECHNICAL PROGRESS | 2 |
| 1. Thermochemistry of Seed and Slag. | 2 |
| 2. Electrical Conductivity and Polarization. | 11 |
| 3. Corrosion of Downstream MHD Components. | 21 |

I. SUMMARY OF PROGRESS TO DATE

1. Thermochemistry of Seed and Slag

Vapor pressure data of K(g) over two $K_2O-CaO-Al_2O_3-SiO_2$ samples are reported. Pressures over these compositions are orders of magnitude greater than over a sample containing roughly the same amount of K_2O but lacking CaO .

Low temperature melting compositions in the quaternary system were determined.

2. Electrical Conductivity and Polarization

The electrical conductivity of a slag containing 20% iron by weight has been completed. The data reinforces the suggestion that the primary conducting mechanism in iron-containing slags at high temperature is iron ion conductivity. A paper giving the information leading to this conclusion was presented at the 7th International Conference on MHD Electrical Power Generation, held at MIT, Cambridge, Mass., June 16 - 20, 1980.

A description of the conductivity measurement technique which was developed over the past year in order to obtain the data is given.

3. Corrosion of Downstream Components

Type 316 and Type 304 stainless steel tubes were exposed for 4 hours to various oxygen/fuel ratios and K_2SO_4/K_2CO_3 seed combinations. These data indicate that seed could cause tube fouling; fouling extent differs under the various test conditions. Wastage evaluations, started last quarter, indicate that Type 304 stainless steel corrodes (weight loss) at the rate of about 4 mm per year.

II. DETAILED DESCRIPTION OF TECHNICAL PROGRESS

I. Thermochemistry of Seed and Slag-(E. R. Plante and L. P. Cook)

A. Vaporization Studies (E. R. Plante)

Measurements of the K and O_2 vapor pressure on two $K_2O-CaO-Al_2O_3-SiO_2$ samples were completed. As in prior work, vapor pressures were determined using a Knudsen-effusion, modulated beam mass spectrometric method.

Both samples consisted of mechanical mixtures of potassium aluminosilicates with calcium silicates or calcium aluminosilicates. Samples have been selected partly on the basis of their phase-equilibrium behavior and partly in order to be able to vary the composition variables to determine their effect on the K_2O activity. For this work, it is advantageous if vaporization of K and O_2 takes place from a homogeneous melt so that the bulk wt% K_2O is an appropriate composition variable. Since the vapor pressure of the other component oxides (CaO , Al_2O_3 , SiO_2) is low or their activity in the condensed phase is low, only the K_2O component was vaporized to any appreciable extent during the current measurements.

Table 1 lists the sample designations, mineral components and starting compositions for the two samples in which measurements have been completed, KCAS-VP-1 and KCAS-VP-2. Similar data for KCAS-VP-3 on which measurements are just beginning are also included.

During the vaporization measurements, the K_2O composition for KCAS-VP-1 varied from its initial value of 14.8 wt% K_2O to a final value of 1.6 wt%. Within experimental error this corresponds closely with the complete vaporization of K_2O from the sample. The measurements on KCAS-VP-2 covered the K_2O composition range from 11.5 to 6.2 wt% at which point they were terminated because a small droplet of sample lodged in the orifice. Because sample preparation involves use of carbonates, residual CO_2 dissolved in the sample at high temperature is expelled with considerable force leading to sample spattering within the Knudsen cell. Some of the vapor pressure data obtained are shown in figures 1-4 and discussed in more detail below.

Vapor pressures of K(g) from the KCAS-VP-1 sample over the range in which the composition varied from 14.8 to 12.4 wt% K_2O are shown in figure 1. The line shown through the experimental points was obtained by least squares without regard to the change in composition of the condensed phase.

It should be noted that there is quite good linearity in the data over the range of the experiment even though the sample below the temperature at which a liquid phase first forms (1310 °C), consists of a mixture of mineral oxides. However, there is a slight increase in the K pressure leading to positive deviation from the linear plot as the temperature is increased above the melting point. At this point in the experiment, the major part of the K_2O is combined in the mineral $KAlSiO_4$, and this observation suggests that the effect of CaO on the K_2O activity at high concentration of K_2O (~ 30 wt% in $KAlSiO_4$) is quite small. The lower line in figure 1 shows the K pressure over a sample obtained from $KAlSiO_4$ in which the K_2O composition was reduced by vaporization to

14.7 wt% K₂O. Although the concentrations of SiO₂ and Al₂O₃ are significantly higher (46.1 and 39.1 wt%, respectively) than in the KCAS-VP-1 sample they are in reality reduced somewhat by an indeterminate amount because of the presence of crystalline mullite. Yet, the K pressure over the calcia containing sample is 250 times higher, which is indicative of the large increase in K₂O activity due to the presence of CaO. Figure 2 shows the last series of data using the KCAS-VP-1 sample. The straight line through the points was fit using data in the composition range 4.8-4.0 wt% K₂O. The additional points show the rapid decrease in K pressure as the K₂O content becomes depleted. The upper curve shows the original K pressure in the 14.8-12.4 wt% K₂O range while the lower curve shows the data for the KAlSiO₄ sample depleted to 14.7 wt% K₂O. Comparison of pressures is a little tenuous for this case because of the difference in slopes. At 1625 K ($10^4/T = 6.25$) the pressure of K has decreased to about 0.1 that in the original sample but is still 36 times greater than that of the 14.7 wt% K₂O sample derived from KAlSiO₄.

Figure 3 is a comparison between the KCAS-VP-1 data in the 14.8-12.4 wt% K₂O range, the KCAS-VP-2 data in the 11.4-10.7 wt% K₂O range and the 14.7 wt% K₂O sample obtained from evaporation of K₂O from KAlSiO₄. At 1625 K the KCAS-VP-1 pressure is 4.5 times greater than that of the KCAS-VP-2 data, which in turn is 65 times greater than the KAlSiO₄ pressure. Reference to Table 1 shows that the KCAS-VP-1 sample initially has about ten percent greater CaO content and ten percent less Al₂O₃ content than the KCAS-VP-2 sample. The higher pressure over the KCAS-VP-1 sample is consistent with its higher K₂O content and the expected behavior of CaO in increasing the K₂O activity.

Figure 4 shows a comparison between the KCAS-VP-2 pressure data in the 6.5-6.2 wt% K₂O range, the 11.4-10.7 wt% K₂O range and the 14.7 wt% K₂O sample obtained from evaporation of KAlSiO₄. At 1625 K, the pressure of the 11.4-10.7 wt% solution is 2.8 times that of the 5.5-6.2 wt% K₂O range while the pressure of the 6.5-6.2 wt% K₂O solution is 22 times that of the 14.7 wt% K₂O sample derived from KAlSiO₄.

While the pressure of K above a solution containing K₂O, CaO, Al₂O₃ and SiO₂ will depend on the concentration of each of the component oxides the major effect of CaO appears to be that of increasing the K₂O activity at lower K₂O concentrations.

Table 2 lists the experiment identification, K₂O concentration range, the slope and its standard error and the intercept and its standard error when the K pressure is fitted to the equation:

$$\log P = A/T + B \quad .$$

It appears that the first two slopes of the KCAS-VP-1 series and the first slope of the KCAS-VP-2 series differ from the remaining slopes which average out to be 16800 ± 500 . At the present time, it is not certain whether the changes in slope are due to the gradual formation of solutions from the original mineral constituents or result from ignoring the change in K₂O composition during the experiments. However, this data requires further analysis and appears in this report primarily as a matter of record.

Table 1

Mineral Constituents and Composition of Vaporization Samples

| Sample | Mineral Constituents | Composition, wt% | | | |
|-----------|--|------------------|------|--------------------------------|------------------|
| | | K ₂ O | CaO | Al ₂ O ₃ | SiO ₂ |
| KCAS-VP-1 | KAlSiO ₄ , Ca ₂ SiO ₄ Ca ₃ Si ₂ O ₇ , Ca ₂ Al ₂ SiO ₇ | 14.8 | 27.5 | 22.2 | 35.5 |
| KCAS-VP-2 | KAlSiO ₄ , KAlSi ₂ O ₆ Ca ₂ Al ₂ SiO ₇ , CaAl ₂ Si ₂ O ₈ | 11.5 | 17.6 | 33.7 | 37.2 |
| KCAS-VP-3 | KAlSiO ₄ , CaSiO ₃ | 14.8 | 24.3 | 16.0 | 44.9 |

Table 2

Tabulation of Slope and Intercept Data for K Pressure Data

| Expt. Id. | wt% K ₂ O | A | σ_m | β | σ_β |
|-----------|----------------------|--------|------------|---------|----------------|
| KCAS-VP-1 | | | | | |
| 3-13-80 | 14.8-12.4 | -20047 | 391 | 8.144 | .255 |
| 3-14-80 | 12.4-9.3 | -19071 | 524 | 7.278 | .334 |
| 3-18-80 | 9.3-7.2 | -17429 | 452 | 6.058 | .289 |
| 3-18-80 | 6.2-4.8 | -16372 | 210 | 5.068 | .129 |
| 3-21-80 | 4.8-4.0 | -16896 | 279 | 5.289 | .178 |
| KCAS-VP-2 | | | | | |
| 5-14-80 | 11.4-10.7 | -14632 | 434 | 4.200 | .278 |
| 5-15-80 | 10.7-8.6 | -16366 | 180 | 5.097 | .112 |
| 5-16-80 | 8.6-6.5 | -17571 | 257 | 5.656 | .158 |
| 5-19-80 | 6.5-6.2 | -16606 | 526 | 4.992 | .321 |

B. Phase Equilibrium Studies in the System $\text{CaO-K}_2\text{O-Al}_2\text{O}_3\text{-SiO}_2$
(L. P. Cook)

The Determination of low temperature melting compositions within the quaternary system continued. Results are shown in Table 3 below.

Table 3

Approximate Compositions (in mole %) of Binary Invariant Melts
Within System $\text{K}_2\text{O-CaO-Al}_2\text{O}_3\text{-SiO}_2$

| | |
|---|-------|
| $\text{KAlSiO}_4/\text{CaSiO}_3$ | 35/65 |
| $\text{KAlSiO}_4/\text{CaAl}_2\text{Si}_2\text{O}_8$ | 19/81 |
| $\text{KAlSiO}_4/\text{Ca}_2\text{Al}_2\text{SiO}_7$ | 37/63 |
| $\text{KAlSiO}_4/\text{Ca}_2\text{SiO}_4$ | 17/83 |
| $\text{KAlSi}_2\text{O}_6/\text{CaSiO}_3$ | 39/61 |
| $\text{KAlSi}_2\text{O}_6/\text{Ca}_2\text{Al}_2\text{SiO}_7$ | 43/57 |
| $\text{KAlSi}_2\text{O}_6/\text{CaAl}_2\text{Si}_2\text{O}_8$ | 30/70 |

Plans: Extend K pressure measurements to additional compositions in the $\text{K}_2\text{O-CaO-Al}_2\text{O}_3\text{-SiO}_2$ system. Attempt to establish correlations of the effect of components on the K_2O activity. Phase equilibrium studies in the $\text{CaO-K}_2\text{O-Al}_2\text{O}_3\text{-SiO}_2$ system will be continued.

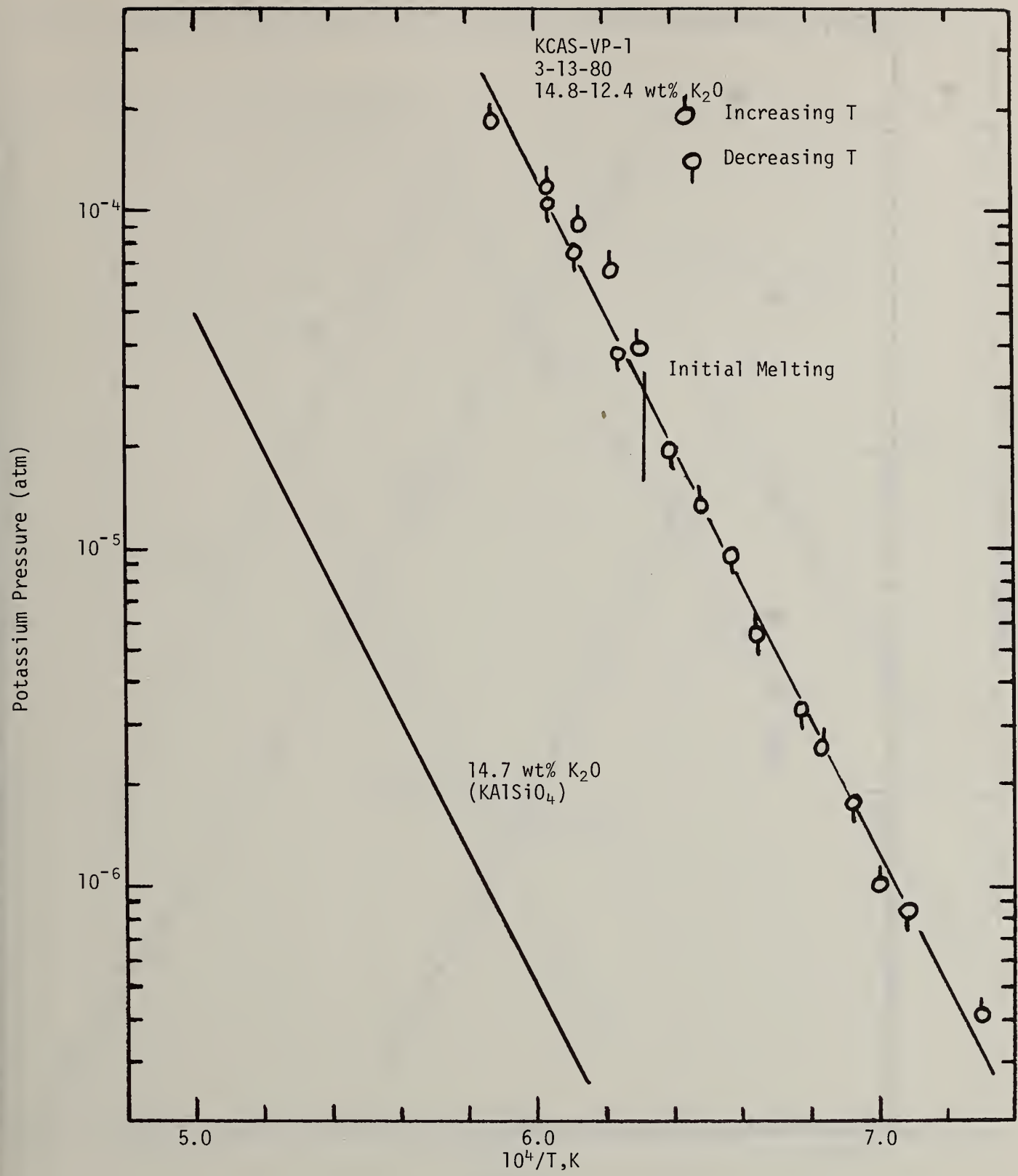


Figure 1 Potassium pressure over KCAS-VP-1. Series 3-13-80, 14.8-12.4 wt% K₂O. Note slight positive deviation from straight line in pressures observed above the initial melting point. Comparison curve pressure from a sample initially consisting of KAlSiO₄, whose K₂O composition has been reduced to 14.7 wt% K₂O by vaporization.

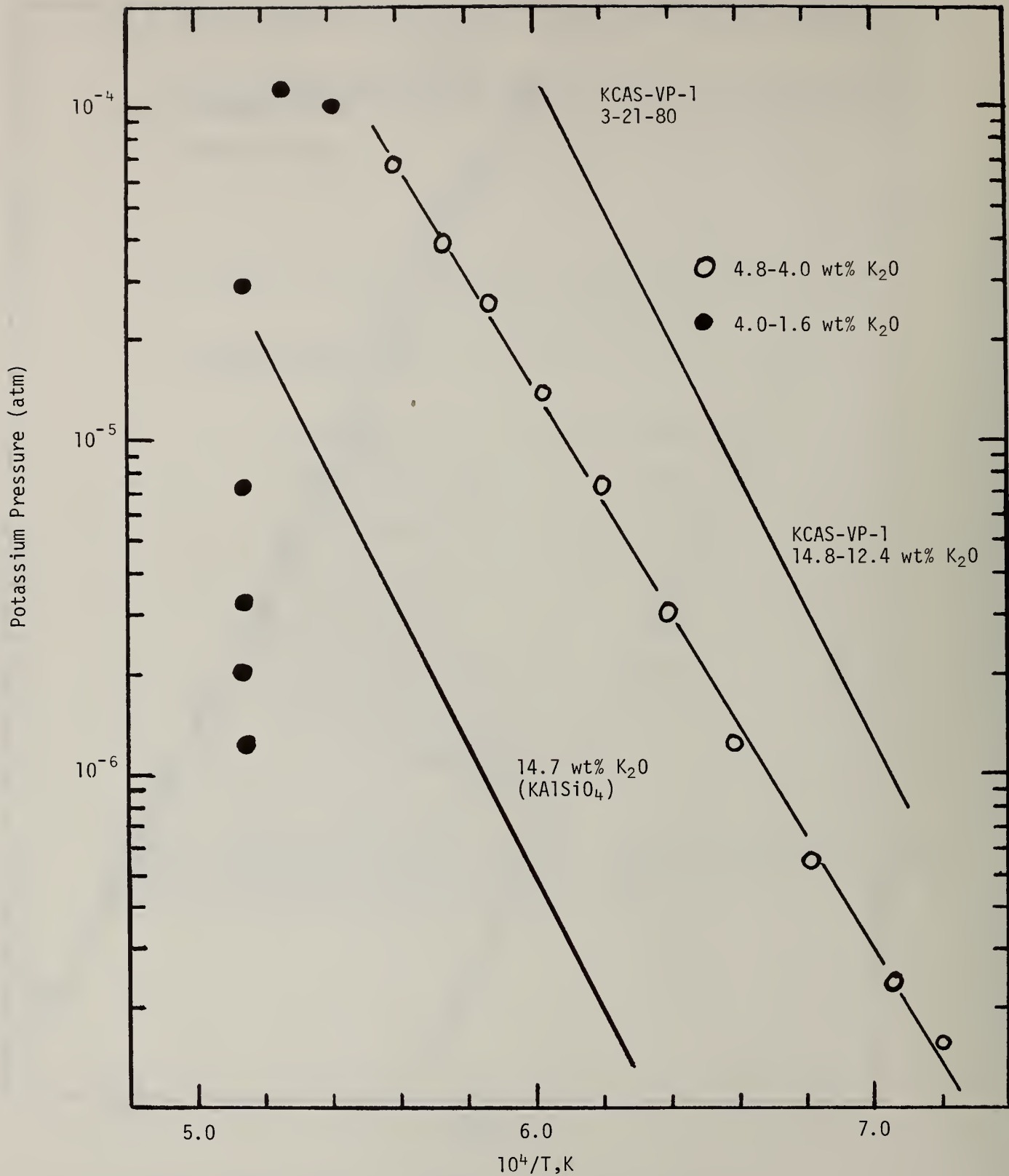


Figure 2 Potassium pressure over KCAS-VP-1. Series 3-21-80, 4.8-4.0 wt% K_2O (straight line plot) followed by pressures from 4.0-1.6 wt% K_2O as K_2O is depleted from the sample. Comparison curves: Upper curve, K pressure with 14.8-12.4 wt% K_2O ; Lower curve, $KA1SiO_4$ depleted to 14.7 wt% K_2O .

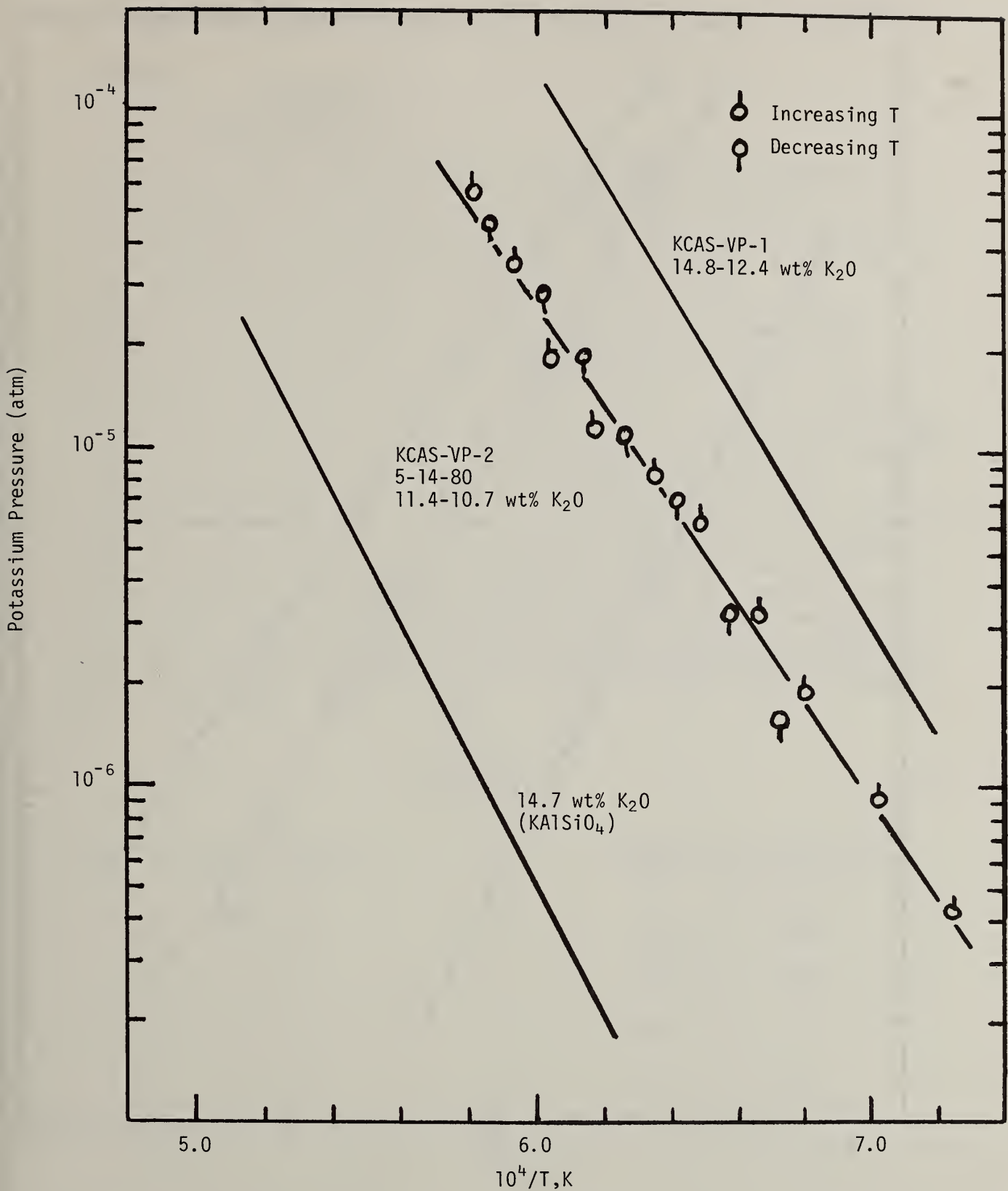


Figure 3 Potassium pressure over KCAS-VP-2. Series 5-14-80, 11.4-10.7 wt% K_2O . Compared with KCAS-VP-1 pressures, 14.8-12.4 wt% K_2O and $KAlSiO_4$ depleted to 14.7 wt% K_2O .

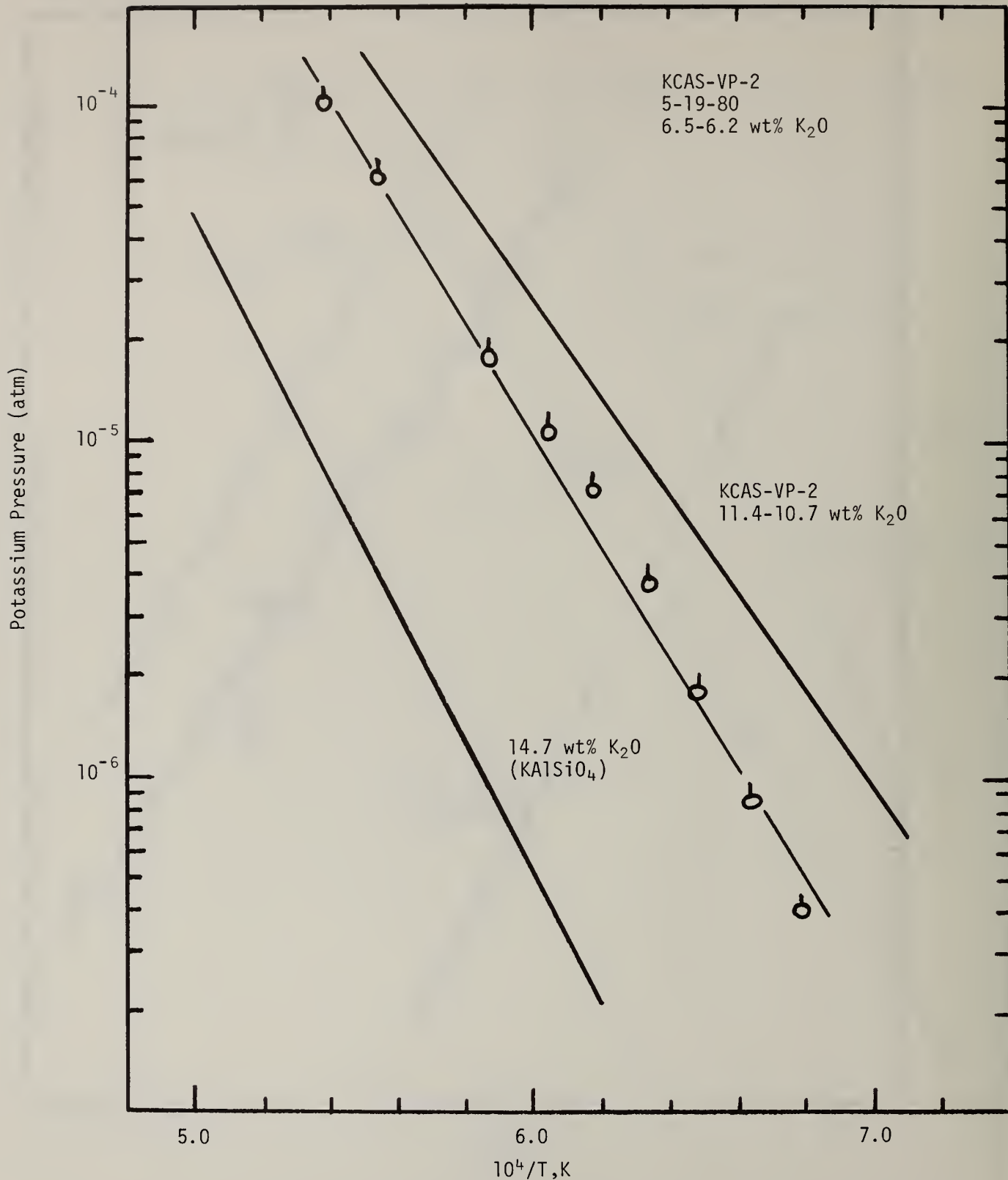


Figure 4 Potassium pressure over KCAS-VP-2. Series 5-19-80, 6.5-6.2 wt% K₂O. Compared with KCAS-VP-2, 11.4-10.7 wt% K₂O and KAlSiO₄ depleted to 14.7 wt% K₂O.

2. Electrical Conductivity and Polarization (W. R. Hosler)

Progress

Slag Electrical Conductivity

In order to further investigate the effect of iron on the electrical conductivity of coal slag in relationship to other slag components, and in relationship to the redox conditions surrounding the material, an additional batch of slag from the Bow, NH steam generating plant (but containing extra iron) has been prepared. Iron was added in the form of Fe_3O_4 to bring the total iron content to 20 mass percent. This material is difficult to form in the measuring crucible and must be formed in a reducing atmosphere before contacts are attached. (See below for an explanation of contacting procedure and four probe DC measurements.) The conductivity measurements on this material have been completed and the data is given in Figures 1 and 2. As in all previous measurements on this slag, there is a break point in the curve above 1385°C ($1/T(\text{K}) \approx 6 \times 10^{-4}$) and all samples show nearly the same slope of conductivity vs. reciprocal temperature regardless of the iron or potassium content and regardless of the ambient oxygen pressure. It is evident, however, that the magnitude of the conductivity in this temperature range is larger than for the data on Bow, NH slag reported in previous quarterly reports beginning April - June 1979 except for that slag sample containing an even larger amount of iron (23.4%) reported in the last quarterly report Jan. - March 1980. Table 1 gives the conductivity at 1450°C of all the samples measured to date. The analyses shown are based on the original analysis of this slag as received from the Bow, NH steam plant. This original analysis is given in Table 1, page 33 of QR April - June 1979.

Table 1

| Based on Initial Analysis | | Conductivity At 1450°C | |
|---------------------------|----------|--------------------------------------|--------------------|
| Mass % Fe | Mass % K | Air | 5 ppm O_2 |
| 14.7 | 0.43 | 0.066 | 0.062 |
| 12.8 | 8.4 | 0.058 | 0.066 |
| 23.4 | 7.5 | 0.31 | |
| 20.0 | 0.40 | 0.16 | 0.16 |

The data shown in Figures 1 and 2 show the same general characteristics below 1385 °C as the previous data on this slag shown in QR April - June 1979 when the data is taken according to a prescribed routine which was designed to freeze in a specific ratio of iron ions ($\text{Fe}^{2+}/\text{Fe}^{3+}$) below 1000 °C. The previous sample contained only 14.7% iron and the conductivity on the lower branch of the conductivity curves (below 1000 °C) is about an order of magnitude lower than for the data shown in Figure 1. The high conductivity branch of the curves, however, are similar in magnitude as well as shape. A preliminary investigation using SEM analyses of these branches of the curves (below 1000 °C) indicates that the conductivity is not primarily a function of the $\text{Fe}^{2+}/\text{Fe}^{3+}$ ratio frozen in by the quench to 900 °C (see QR April - June 1979) but is due mostly to the crystalline component of the solidified slag. Scanning electron microscope micrographs show crystallite bridging in various degrees depending on the history of the sample. It is possible that this bridging accounts for the somewhat unpredictable conductivity below 1000 °C particularly since there does not seem to be a primary dependence of the conductivity on the oxygen pressure (vis. Fig. 1 and 2). This concept is being investigated and will be reported on at a later time. A paper was presented at the 7th International Conference on MHD, held at MIT in Cambridge, June 16 - 20, 1980, Session 5, Paper No. D - 7 which gives a possible explanation for the high temperature behavior (above 1385 °C) of iron-containing slags. It can readily be seen from Table 1 that the conductivity at 1450 °C depends on the iron content and not on the amount of potassium (for the several amounts shown in the table) and not on the oxygen partial pressure in the range from 0.2 to 10^{-6} atmospheres. The conclusion drawn then is that for this slag composition, the conductivity above 1385 °C is due primarily to the iron ions.

Measurement Technique and Sample Preparation

Measurements of the physical properties of materials at high temperatures are becoming increasingly important particularly with respect to emerging energy technologies. A few examples include materials used in magneto-hydrodynamics, fuel cells, and batteries for energy storage and conversion of chemical to electrical energy. The electrical conductivity of some materials for these technologies is important as all require the passage of current (ionic and/or electronic). For those materials that remain solid with relatively simple chemistry in a device, the conductivity measurement over the useful temperature range is not difficult. However, for those materials that may be in a solid and/or liquid state, depending on temperature, the measurement becomes more difficult. Measurements are complicated further by chemical interaction of a material with the containing crucible, by chemical/phase changes with temperature and oxygen pressure, by thermal expansion or contraction problems upon solidification or cooling, and by the requirement of electrical contacts that will give reliable results without disintegration. A measurement technique has been developed over the last year which can alleviate these problems. A brief description of the sample preparation and measurement technique both of which are extremely important for obtaining valid results on high temperature materials such as coal slag follows.

Generally, only four probe DC conductivity measurements will be discussed. Two probe DC measurements give erroneous results when ionic conductivity is involved, especially when ion exchanging electrodes are not used. AC measurements are useful for samples having relatively high resistances where capacitive reactance components can be determined at reasonable frequencies (< several megahertz). For most high temperature materials, however, the electrical conductivities are high enough (~ 0.01 to $10 \text{ ohm}^{-1}\text{cm}^{-1}$) so that the required frequencies are too high to resolve the capacitive-reactive components of the total impedance which are due to contact barrier layers or grain boundary effects. Four probe AC measurements, however, are a viable option but usually require more instrumentation than DC measurements.

For materials which can be cut to a suitable sample size and will not flow over the temperature range of the measurement, contacts can be applied directly to the material by drilling small holes (using a diamond dental drill) in the sample to attach the contact lead wires. This is done by peening spongy platinum around the leadout wires, which are usually platinum to withstand the high temperature oxidizing atmospheres. A schematic diagram of a typical contact is shown in Figure 3. Generally the portion of the wire in the hole should have a non-symmetrical configuration on the end to prevent the wire from turning in the hole and to prevent pull-out from the adjacent peened platinum. In the schematic, an oval disk is shown. This was made by inserting the leadout wire with a small ball on the end through a hole in a piece of metal and simply hammering the ball flat. Any non-symmetrical shape formed in any way will suffice. Measurements using this contacting method have been made on many ceramic materials up to $1700 \text{ }^\circ\text{C}$. No contact resistances were apparent. For best results, the materials should be fully sintered up to the highest measuring temperature to prevent further densification during measurement. Figure 4 shows a radiograph of a sample of $\text{Y}_{0.95}\text{Ca}_{0.05}\text{CrO}_3$ with contacts applied as described above.

For a material such as slag that becomes molten within the range of temperatures involved in the measurement, a different procedure was used. Alumina crucibles which are readily available and which show minimal reaction with the slag were chosen for the experiments. A crucible is carefully filled to just under one-half full by repeated melting of additions of slag powder. This is necessary to prevent the material with absorbed gases from bubbling over the top during the initial filling process. Holes are then drilled through the crucible sides and into the slag for the four probes. Leads are attached using the same procedure as described above. Figure 5 shows a radiograph of a typical crucible with leads attached and numbered for the discussion to follow.

Spongy platinum is commercially available from several companies specializing in platinum products. It can readily be made, however, from powdered platinum which is sintered lightly at $1200 \text{ }^\circ\text{C}$ for 1/2 hour. The resulting spongy solid mass can be cut into pieces and can be pressed into the holes surrounding the leadout wires. For small samples such as described above, the contacting must be done under a binocular

microscope. The peening tools can be made from any hardened metal material formed into a suitable tip for compaction of the spongy platinum. This method yields a leak-tight seal.

It can be seen (Fig. 5) that the size and shape of the molten sample remains fixed during the course of the measurement. This is essential for accurate determination of a conductivity. Furthermore, the electrodes do not penetrate a surface exposed to the ambient atmosphere so that oxidation-reduction conditions at the surface do not affect the conductivity value.

The measurements are made using a constant current power supply. In certain temperature ranges and under certain conditions the material is an ionic conductor. Under these circumstances, care must be taken during data acquisition to avoid polarization on the conductivity probes (two center probes). Since the current is maintained constant, the voltage measured between the conductivity probes is a true measure of the bulk conductivity of the material, i.e., $\sigma = 1/\rho = \lambda I/AV_{23}$ where A is the cross sectional area of the sample, λ is the distance between the conductivity probes 2 and 3, and V_{23} is the potential developed between the conductivity probes 2 and 3 at a constant current I . This conductivity may be electronic and/or ionic depending on the chemical (bulk and phase) and physical state of the material, but V_{23} will remain constant with time. If there is no potential drop at the current contacts (contacts 1 and 4, Figure 5) due to a contact resistance and the conductivity is entirely electronic, no polarization with time will be observed at a given temperature on all probe sets V_{12} , V_{23} , V_{34} , or V_{14} . If the conductivity is ionic or partially ionic and probe measurements are taken in a reasonably short time at low electric fields ($< 1\text{V/cm}$) such that polarization effects do not extend far beyond the current carrying contacts 1 and 4, probe voltage V_{23} will remain constant but V_{12} , V_{34} and V_{14} will change with time during the short interval that current is flowing for the measurement. With the data acquisition system (D.A.S.) used in this experiment, collecting a set of data points (i.e., V_{12} , V_{23} , V_{34} , V_{14} , temperature, current, and time) required about 40 seconds for one applied voltage polarity. Since the current is reversed for each data point at a given temperature to eliminate permanent polarization build up at any current carrying electrode and to eliminate any thermoelectric voltage present due to a temperature gradient along the length of the sample, the total time to scan all voltages for both current directions is approximately 80 seconds. The D.A.S. consists of a programmable calculator-based system interfaced with appropriate electrometers and voltmeters to measure the necessary parameters. The data can be stored and calculations are made automatically after the current is off.

All conductivity curves reported during the last year were obtained using this method. These are a reflection of the probe voltage V_{23} versus the temperature. Each point on the curve is representative of near equilibrium conditions for temperatures above 1000°C . Since diffusion of oxygen is relatively slow at temperatures below 1000°C ,

very long times are required, days or weeks, for complete stabilization and data below this temperature have a quenched in $\text{Fe}^{2+}/\text{Fe}^{3+}$ ratio and crystalline content. In addition, for slag samples, precipitation and re-resolution of crystalline phases causes the conductivity to change with time at a given temperature above 1000 °C. These processes generally follow an exponentially decreasing curve. In order to be able to complete the experiment in a reasonable time, a data point was considered close enough to its final equilibrium value when the change in conductivity was less than 1% over a ten minute period. At a given temperature, data was taken at ten minute intervals with applied voltage off between measurements. Above 1300 °C these conditions could be met in less than 1 hour while below 1300 °C times as long as 20 hours were required. No polarization was observed in this voltage measurement (V_{23}) at any time during the run. Since polarization at current carrying contacts can be expected for ionic conductors where the electrodes are not ion exchanging, as is the case here, some information can be obtained by comparing the voltages developed at the probe sets during the course of the data acquisition. A complete description of the information that can be obtained in this manner will be given in a later quarterly report. For best results these scan voltages must be interpreted in conjunction with x-ray diffraction and scanning electron microscope analytical techniques.

Plans

Electrical conductivity measurements of various slags will continue with particular attention to analysis of the results pointing closely to understanding the conductivity process. The analytical methods described in this report will be extended and hopefully will be applied to four probe AC conductivity data if the equipment on hand will lend itself to this measurement.

In the last quarterly report, an electrochemical study was reported on a slag at 1250 °C. This temperature is below the break point in conductivity (1385 °C) as shown in Figures 1 and 2 of this report on slag containing no added potassium. Voltage breakdown was seen to occur at this temperature (1250 °C) in about 2 minutes in a constant current mode at a current density of 0.2A/cm². This experiment should be repeated at a temperature greater than 1385 °C to determine the effect of decreased viscosity and hence, increased iron ion conductivity of slag on the time for voltage breakdown.

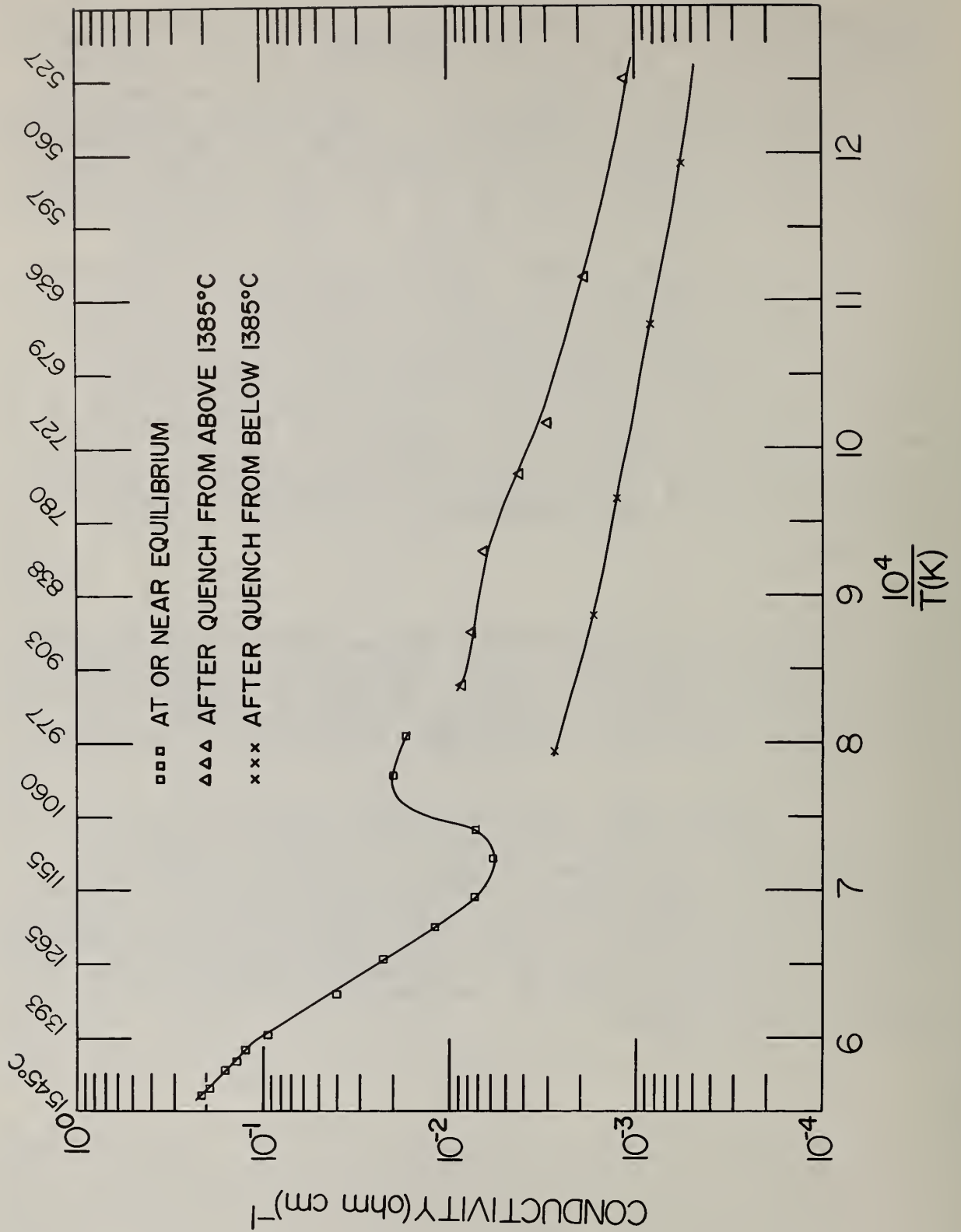


Figure 1. Electrical Conductivity of Bow N.H. slag containing 20 % Fe as a function of temperature in an air atmosphere.

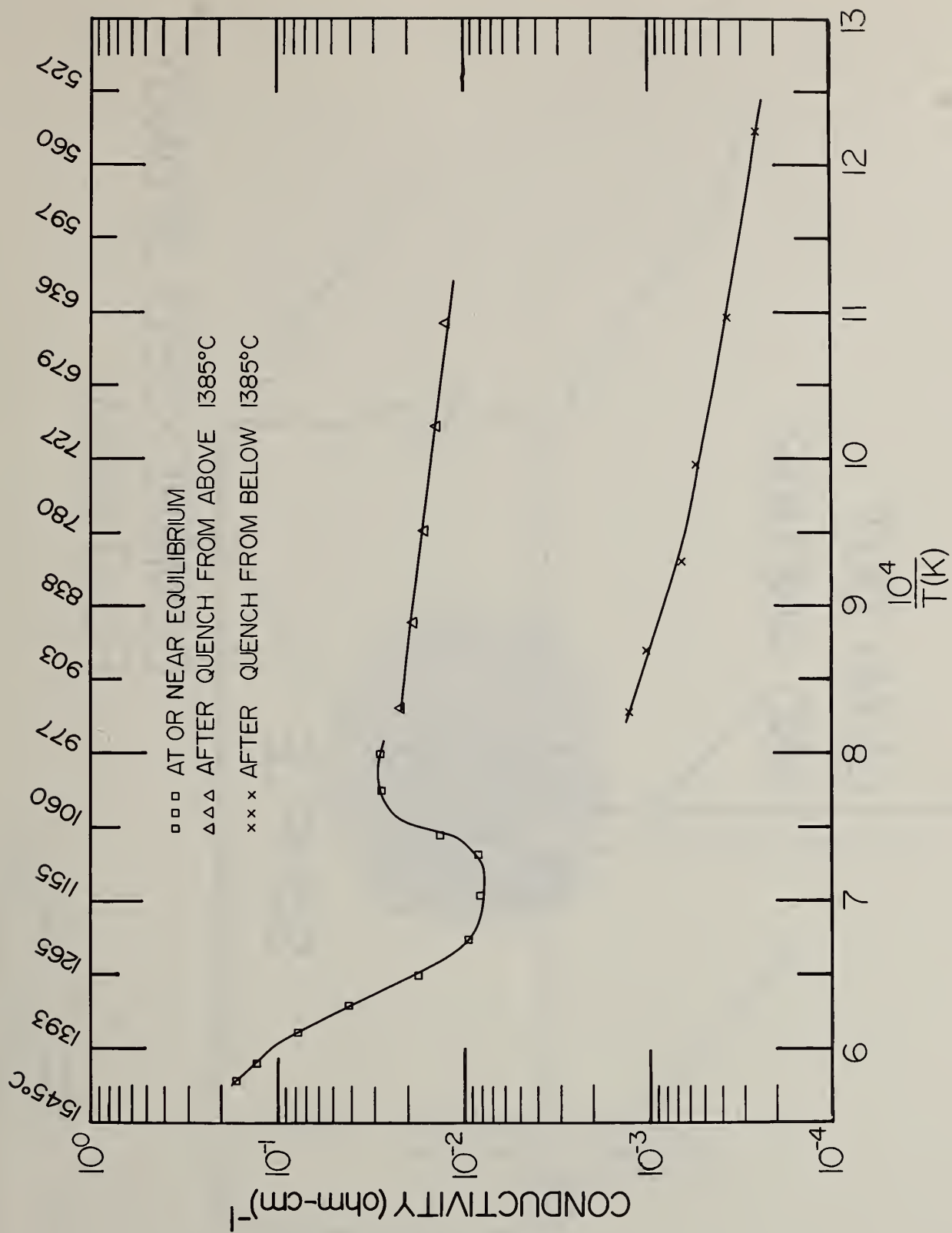


Figure 2. Electrical conductivity of Bow NH slag containing 20 % Fe as a function of temperature in an atmosphere of 5×10^{-6} ppm O_2 in N_2 .

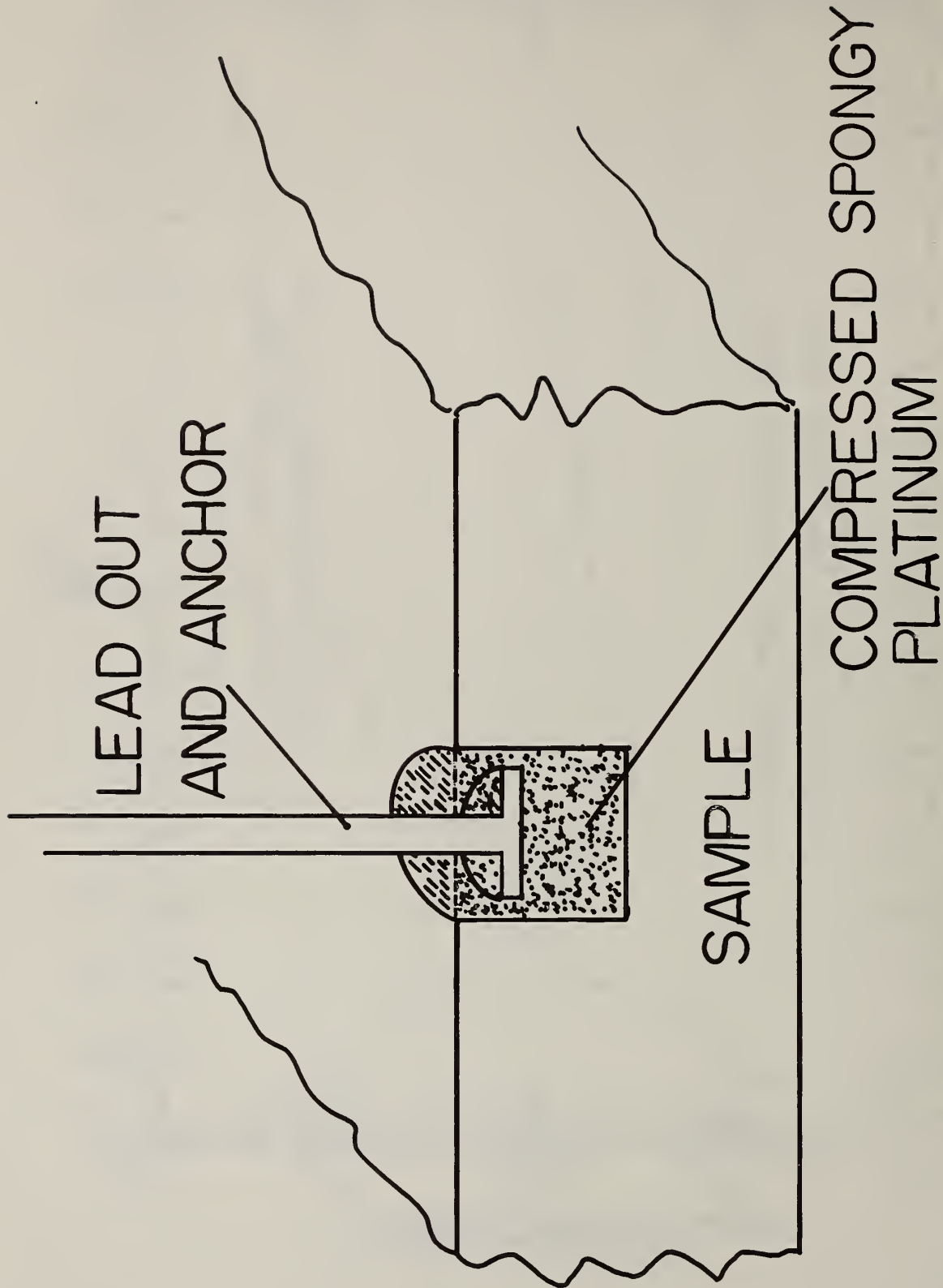


FIGURE 3. Schematic of typical leadout wire assembly for high temperature electrical conductivity measurements

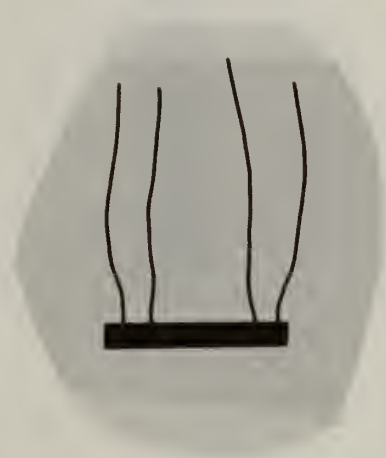


FIGURE 4. Radiograph of sample and leadout wires mounted as illustrated in Fig. 3

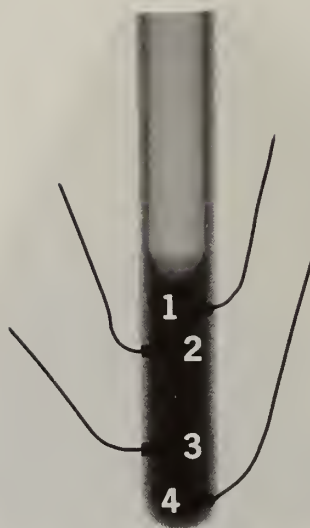


FIGURE 5. Radiograph of slag sample contained in alumina crucible with leadout wires (numbers) extending through walls

4. Corrosion of Downstream MHD Components (J. Smit and C. D. Olson)

Progress: Type 316 and Type 304 stainless steel tubular specimens were exposed to seeded oxygen-propane fired hot gas streams at various seed compositions, fuel to oxygen ratios and tube wall temperatures. Exposure time for all specimens, exclusive of apparatus warm-up and cool-down time was four hours. Seeding took place for the first twenty-five minutes of exposure during which approximately 250 grams of seed was added to the hot gas stream. For all specimens the gas stream temperature in the vicinity of the specimen was held at about 1300 °C. Tube wall temperatures, monitored by Pt/Pt10Rh thermocouples welded into the midpoint of the specimens, were maintained at either 500 °C or 590 °C by internal air cooling.

Six specimens of Type 316 stainless steel were exposed in the manner described above and to the specific conditions as indicated in Table 1.

Table 1.

| <u>Specimen No.</u> | <u>Wall Temp. (°C)</u> | <u>Seed</u> | <u>Gas Stream State</u> |
|---------------------|----------------------------|-----------------------|-------------------------|
| 5-6 | 500 | K_2SO_4 | fuel rich |
| 6-6 | 590 | K_2SO_4 | fuel rich |
| 7-6 | 500 | $K_2SO_4 + K_2CO_3^*$ | O_2 rich |
| 8-6 | 590 | $K_2SO_4 + K_2CO_3^*$ | O_2 rich |
| 9-6 | 590 | $K_2SO_4 + K_2CO_3^*$ | fuel rich |
| 10-6 | 500 | $K_2SO_4 + K_2CO_3^*$ | fuel rich |

* Ratio of K_2SO_4 to K_2CO_3 is 1:4 by weight.

Following exposure, sections were taken from the specimens for optical, SEM and EDX analysis. The sections, prepared using metallographic techniques, were cut from a location 10 mm away from the midpoint position on the specimen. Because of the sensitivity of the deposited coatings to moisture the tubular specimens were encapsulated immediately upon removal from the test rig. All cutting, grinding, and polishing operations were conducted using non-aqueous media. In addition the sections were stored in vacuum dessicators except during intervals of processing. Figures 1-6 are optical micrographs of specimens 5-6 through 10-6 so handled. The geometry of the deposited coatings is consistent with that observed on the Type 304 stainless steel tubes at the same conditions and reported on previously.

The nature, size and shape of the deposited coatings is of importance to both the heat and seed recovery aspects of the bottoming steam plant operation. These characteristics will effect not only the heat transfer properties of the system but will also have a major influence on fouling conditions particularly in the main heat exchanger. Further, the removal of this material and its subsequent transport downstream will prove an added burden to the seed recovery system.

Figures 7-18 are micrograph of sections of Type 304 stainless steel reported on earlier showing the deposited coatings. The leading surface of a specimen is at the top of each figure. These specimens were prepared in the same manner as the Type 316 stainless steel tubing described in a succeeding paragraph. The conditions of exposure are given in Table 2 and some conclusions regarding these coatings follow.

Table 2.

| <u>Figure No.</u> | <u>Temp. of Tube Wall, °C</u> | <u>Seed</u> | <u>Gas Stream Condition</u> |
|-------------------|-------------------------------|-----------------------|-----------------------------|
| 7 | 400 °C | K_2SO_4 | O_2 rich |
| 8 | 500 °C | K_2SO_4 | O_2 rich |
| 9 | 590 °C | K_2SO_4 | O_2 rich |
| 10 | 400 °C | K_2SO_4 | fuel rich |
| 11 | 500 °C | K_2SO_4 | fuel rich |
| 12 | 590 °C | K_2SO_4 | fuel rich |
| 13 | 400 °C | $K_2SO_4 + K_2CO_3^*$ | O_2 rich |
| 14 | 500 °C | $K_2SO_4 + K_2CO_3^*$ | O_2 rich |
| 15 | 590 °C | $K_2SO_4 + K_2CO_3^*$ | O_2 rich |
| 16 | 400 °C | $K_2SO_4 + K_2CO_3^*$ | fuel rich |
| 17 | 500 °C | $K_2SO_4 + K_2CO_3^*$ | fuel rich |
| 18 | 590 °C | $K_2SO_4 + K_2CO_3^*$ | fuel rich |

* Ratio of K_2SO_4 to K_2CO_3 is 1:4 by weight.

Generally a compact seed deposit forms on the leading surface of the tube, being thinnest at the midpoint and broadest at the compact deposit-powdery deposit merge zone. A thinner somewhat powdery deposit forms on the trailing surface. The leading surface deposit is independent of temperature (400 °C - 590 °C) for the case of K_2SO_4 in O_2 rich hot gas streams. For all other cases the deposit thickness decreases with increasing tube wall temperature. Leading surface deposits are generally thicker in O_2 rich hot gas streams while trailing surface deposits are generally thicker in fuel rich hot gas streams. The combination of K_2SO_4 with K_2CO_3 results in a thinner deposit at all temperatures for the O_2 rich hot gas stream case than for the K_2SO_4 alone.

From the preceding then it may be argued that fouling in the heat exchanger area would probably be least and the heat transfer efficiency greatest at the higher temperature, i.e., above 500 °C, with a $K_2SO_4 + K_2CO_3$ mixture probably in an oxygen rich hot gas stream.

The gravimetric studies initiated in the last quarter were continued during this reporting period. Three specimens of Type 304 stainless steel tube were exposed at 590 °C to conditions indicated in Table 3. Prior to exposure the specimens were cleaned with ethanol and weighed. Immediately following exposure the specimens were rinsed with warm water and then ethanol to remove the seed deposit. The specimens were then cleaned in a ultrasonic bath with 10% HNO_3 at 50 °C for twenty minutes and reweighed. The weight change is noted in Table 3. Even by the most conservative treatment the weight loss translates to a wastage of 4 mm per year which is not acceptable and would virtually eliminate Type 304 stainless steel as a candidate material.

Plans: Specimens of Type 316 stainless steel previously exposed and prepared will be analyzed by SEM and EDX techniques for signs of both incipient and gross corrosion. In addition deposit samples obtained from specimens exposed for gravimetric analysis will be analyzed using x-ray diffractometer techniques. The purpose of this analysis is to obtain more information on the corrosion process involved and on the possible transformation of the seed compounds during deposition.

Table 3.

| Specimen No. | Specimen Stainless Type | Seed | Gas Stream State | Specimen Temp. °C | Weight in Grams Before Test | Weight in Grams After Test | Change in Weight in Grams |
|--------------|-------------------------|---------------------|------------------|-------------------|-----------------------------|----------------------------|---------------------------|
| 15-4 | 304 | K_2SO_4 | fuel rich | 590 | 67.233 | 67.187 | 0.046 |
| 16-4 | 304 | $K_2SO_4 + K_2CO_3$ | fuel rich | 590 | 66.320 | 66.289 | 0.031 |
| 17-4 | 304 | $K_2SO_4 + K_2CO_3$ | O_2 rich | 590 | 66.378 | 66.351 | 0.027 |

Fig. 1. Section of Type 316 stainless steel tubing after exposure to K_2SO_4 seeded fuel rich hot gas stream. Note deposit on lower surface. Tube temperature 500 °C. 6 X.

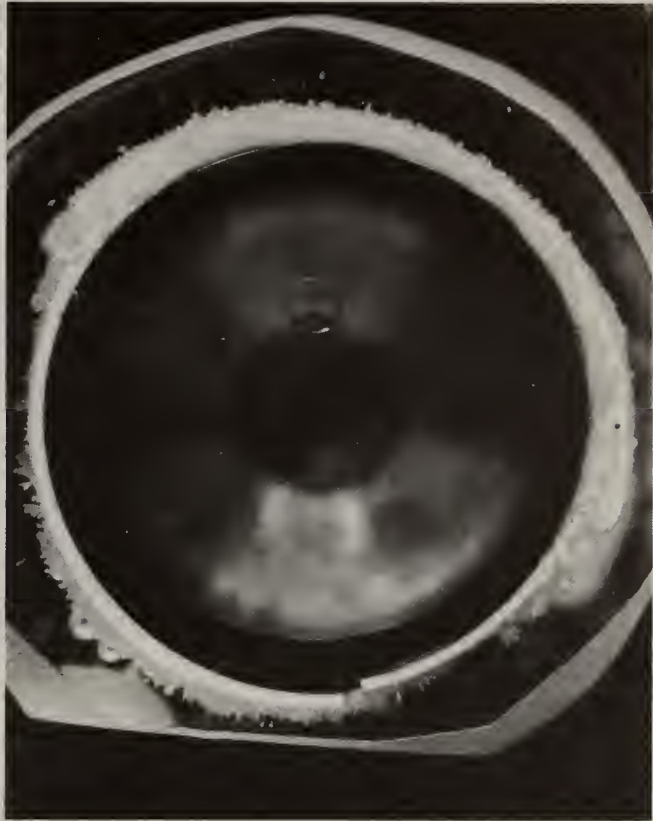


Fig. 2. Section of Type 316 stainless steel tubing after exposure to K_2SO_4 seeded fuel rich hot gas stream. Note thin deposit on upper surface. Tube temperature 590 °C. 6 X.





Fig. 3. Section of Type 316 stainless steel tubing after exposure to $K_2SO_4 + K_2CO_3$ seeded O_2 rich hot gas stream. Note thick deposit on upper surface. Tube temperature $500\text{ }^\circ\text{C}$. 6 X.

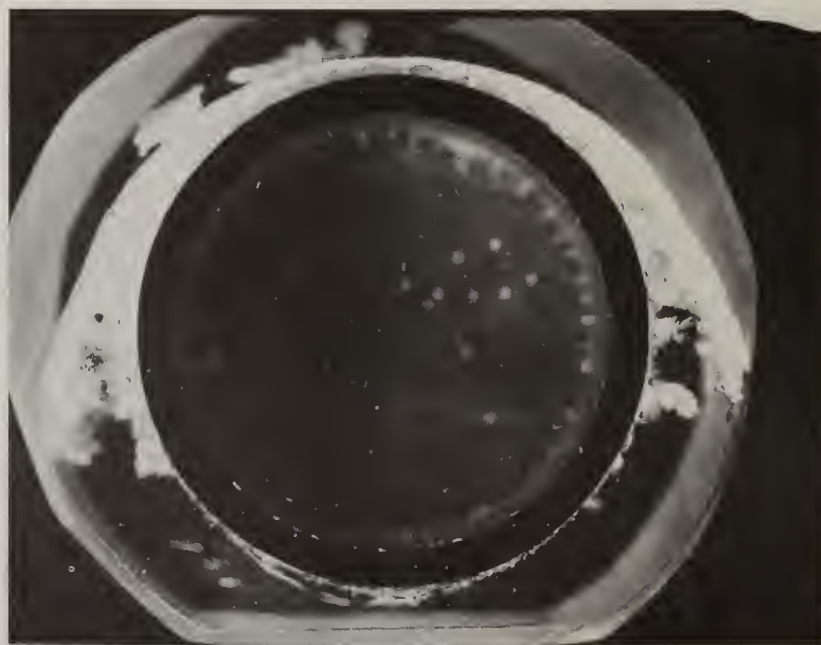


Fig. 4. Section of Type 316 stainless steel tubing after exposure to a $K_2SO_4 + K_2CO_3$ seeded O_2 rich hot gas stream. Tube temperature $590\text{ }^\circ\text{C}$. 6 X.



Fig. 5. Section of Type 316 stainless steel tubing after exposure to a $K_2SO_4 + K_2CO_3$ seeded fuel rich hot gas stream. Note deposit on lower surface. Tube temperature 500 °C. 6 X.



Fig. 6. Section of Type 316 stainless steel tubing after exposure to a $K_2SO_4 + K_2CO_3$ seeded fuel rich hot gas stream. Tube temperature 590 °C. 6 X.



Fig. 7. Section of Type 304 stainless steel tubing after exposure to K_2SO_4 seeded oxygen rich hot gas stream. Note formation of thick deposit, 2 mm, on upper surface and thin powdery deposit on lower surface. Tube temperature 400 °C. 6 X.

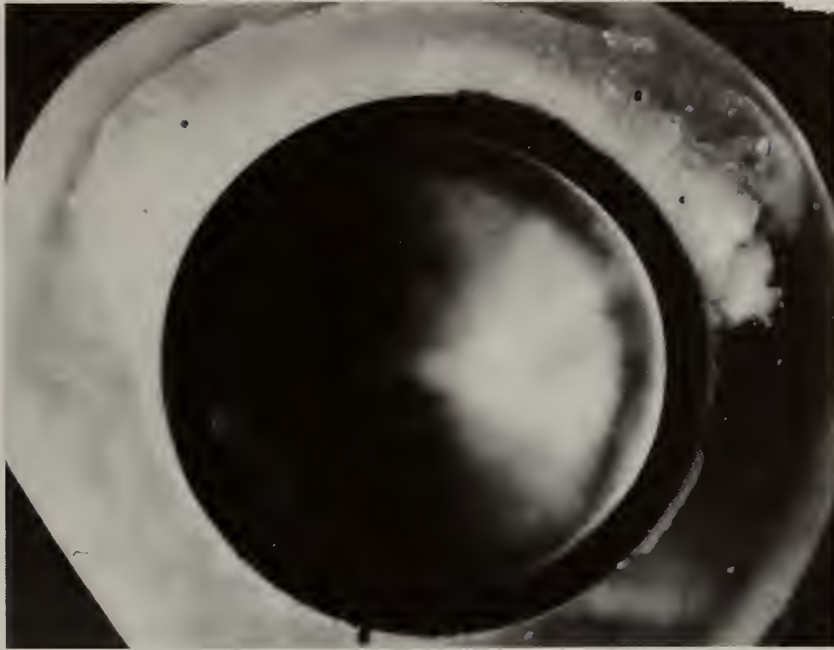


Fig. 8. Section of Type 304 stainless steel tubing after exposure to K_2SO_4 seeded oxygen rich hot gas stream. Note formation of thick, 2 mm deposit on upper surface. Tube temperature 500 °C. 6 X.



Fig. 9. Section of Type 304 stainless steel tubing after exposure to K_2SO_4 seeded oxygen rich hot gas stream. Note formation of thick deposit on upper surface. Tube temperature 590 °C. 6 X.

Fig. 10. Section of Type 304 stainless steel tubing after exposure to K_2SO_4 seeded fuel rich hot gas stream. Tube temperature 400 °C. 6 X.



Fig. 11. Section of Type 304 stainless steel tubing after exposure to K_2SO_4 seeded fuel rich hot gas stream. Tube temperature 500 °C. 6 X.





Fig. 12. Section of Type 304 stainless steel tubing after exposure to K_2SO_4 seeded fuel rich hot gas stream. Tube temperature $590^\circ C$. 6 X.



Fig. 13. Section of Type 304 stainless steel tubing after exposure to $K_2SO_4 + K_2CO_3$ seeded O_2 rich hot gas stream. Note formation of thick, 1.7 mm, deposit on upper surface. Tube temperature $400^\circ C$. 6 X.



Fig. 14. Section of Type 304 stainless steel tubing after exposure to $K_2SO_4 + K_2CO_3$ seeded oxygen rich hot gas stream. Note formation of thick, 1 mm, deposit on upper surface. Tube temperature 500 °C. 6 X.



Fig. 15. Section of Type 304 stainless steel tubing after exposure to $K_2SO_4 + K_2CO_3$ seeded oxygen rich hot gas stream. Note formation of thinner deposit on upper surface. Tube temperature 590 °C. 6 X.

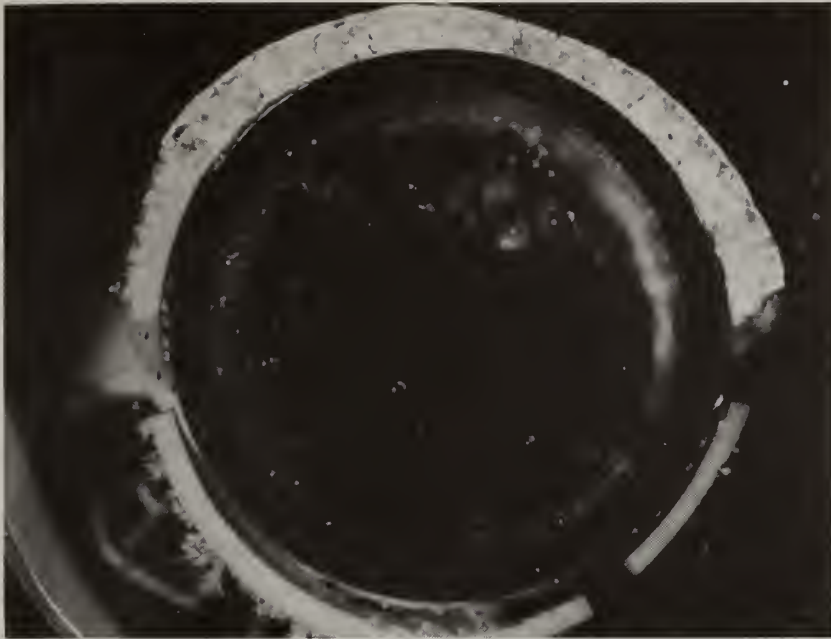


Fig. 16. Section of Type 304 stainless steel after exposure to $K_2SO_4 + K_2CO_3$ seeded fuel rich hot gas stream. Note formation of 0.8 mm thick deposit on upper surface. Tube temperature 400 °C. 6 X.



Fig. 17. Section of Type 304 stainless steel tubing after exposure to $K_2SO_4 + K_2CO_3$ seeded fuel rich hot gas stream. Tube temperature 500 °C. 6 X.



Fig. 18. Section of Type 304 stainless steel tubing after exposure to $K_2SO_4 + K_2CO_3$ seeded fuel rich hot gas stream. Note deposit on lower surface. Tube temperature 590 °C. 6 X.